Adsorption of Cd(II) and Fe(II) Ions by Inorganic Nanocomposites (CuO/ZnO) from Aqueous Solutions

Mohammed Khlaif Challab[1*], Mohammad Javad Chaichi[1], Mohammed Turki Khathi[2], Omleila Nazari[1], and Shahram Ghasemi[1]

[1]Faculty of Chemistry, University of Mazandaran, Pasdaran, Babolsar, Mazandaran 47416-13534, Iran

[2]Department of Chemistry, Faculty of Science, Thi-Qar University, Al-Jadriya, Nasiriyah 64001, Iraq

** **Corresponding author:***

email: mohammadchellab@gmail.com

Received: February 17, 2025
Accepted: April 11, 2025

DOI: 10.22146/ijc.104802

Abstract: *This research aims to investigate the nanocomposite effectiveness from CuO:ZnO-NPs at a 1:1 ratio in water-polluting heavy metals adsorption from aqueous solutions, since these heavy metals adversely affect living organisms, including cadmium and iron. The research also examines the effectiveness of heavy metal removal when influenced by parameters like pH, adsorption dose, contact duration, initial concentration, and temperature. The maximum adsorption efficiency of heavy metals reached 86.7% for Cd(II) and 84.9% for Fe(II) at 25 °C when solution conditions totaled 10 mg/L of heavy metals alongside a pH setting of 6 using 0.09 g of sorbent. The structural and physical properties of the sorbent were analyzed by atomic and FTIR, along with FE-SEM, BET, XRD, and EDX systems. This study aimed to find an economical approach for heavy metal-infused water purification and analyze water quality changes to prove the feasibility of treating these pollutants using sorbent surfaces.*

Keywords: *adsorption; nano-adsorbent; removal; composite; heavy metals*

INTRODUCTION

Water is one of the most essential things because it is the source of human existence and life for creatures on planet Earth. As the need for water increases, water purity faces many difficulties. The development of industrialization, agricultural development, and the expansion of human civilization have led to the aquatic environment being exposed to pollution and change that affects creatures in general. This had led to a negative impact on the vital water bodies used by humans and living ambushes such as rivers and oceans, which affects the health of humans and all creatures on the planet. Environmental pollution has been recognized worldwide and is considered a global issue because it negatively affects all aquatic systems and significantly damages human health and the lives of marine organisms. Therefore, advanced measurement and treatment must be taken to prevent and mitigate the harmful effects of all materials that pollute the environment and water and affect public health [1].

Water pollution has wide-ranging damage and effects on all environmental systems. There is a large group of materials that pollute the environment, including chemical fertilizers, various pesticides, and materials that settle, as well as heavy metals, which are considered a major cause of environmental pollution. The increase in the global population affects and aggravates the level of pollution. The percentage of water on the Earth's surface is about 70%; however, only about 2.5% of this total volume is considered suitable for human use. Groundwater serves as a basic and essential source in rural and urban areas. The expansion of the global population, the diversion of water resulting from domestic activities, and the waste of pharmaceutical factories have exposed groundwater to the risk of contamination. It is estimated that approximately 80% of diseases are waterborne [2].

As is well known, water is the leading and basic resource for the continuation of life for living organisms on the planet. Pollutants that pollute water and the environment are a major and widespread threat. Pollutants that pollute water have been divided into several forms, including inorganic, organic, pathogenic, thermal, and radioactive pollutants. Green nanotechnology is a modern field of scientific studies focusing on biologically manufacturing nanomaterial using biological materials used by living cells [3].

The use of technology that relies on the use of plant extracts for the green synthesis of nanoparticles (NPs) with a size of 1 to 100 nm is better than the old traditional methods due to its advantages and properties that traditional methods lack, such as environmental safety, low toxicity, and excellent economic feasibility. The synthesis of nanomaterial's based on the use of biological waste is one of the modern aspects of nanotechnology. This technology is better due to its advantages and properties, which are cost-effective, safe, environmentally sustainable, and biocompatible, as it uses a plant extract from peanut shells to synthesize Cu/CuO NPs [4].

The synthesis of metal NPs by the green synthesis technique is a plant-based technology due to its simplicity, environmental friendliness, ease of use, and availability of different types of plants that can be used for manufacturing. *Albizia saman* leaf extract was used to synthesize CuO NPs. It was found that the leaf extract contains phenolic and flavonoid compounds. It is effective in the synthesis of CuO NPs. The plant extract from the seeds of the *Caesalpinia pondocella* plant is also used in an environmentally friendly manner. This is due to the seeds containing numerous components, such as citrulline and flavonoids, which play a key and effective role in the manufacturing process as reducing agents. The green synthesis techniques offer cost-effective and environmentally friendly possibilities for manufacturing NPs, especially metal oxides, such as an extract of *Aloe miller* leaf to produce CuO NPs [5].

Albizia odoratissima plant extract was used to produce silver NPs, which served to remove lead(II) and copper(II) ions from aqueous solutions. This method is considered safe, and the plant extract demonstrated significant effectiveness as a reducing agent, with high removal rates. Metal oxide nanocomposites have received wide and significant scientific attention in all environmental fields, including removing or reducing environmental pollution. The composite of CuO and ZnO is of great interest due to its properties and environmental friendliness. These materials increase the surface area, increasing the active sites that work to remove environmental pollutants. An aqueous extract of mangosteen (*Garcinia mangostana* L.) leaves was used to synthesize CuO and ZnO NPs and their nanocomposites (CuO-ZnO NPs). The nanocomposites represent a budget-friendly and earth-friendly material [6].

Adsorption decontamination technology is a very effective method for removing various pollutants from wastewater. The absorbent materials are readily available, suitable, and inexpensive, in addition to being simple to operate and highly efficient in adsorbing pollutants, and they have significant and prominent advantages. The removal and treatment of heavy metals were expensive. Studies and experiments have proven that adsorption technology is very effective due to its great properties in removing and reducing the concentration of heavy metal pollution to very low levels by using many adsorbent materials available in the environment [7].

The contaminated state of water with heavy metals stands as one of today's most severe environmental problems because of rising industrial operations and traditional agricultural methods that lack modern technology. The availability of groundwater over 30% worldwide suffers from critical heavy metal contamination, which includes both Cd and Fe. These metals seriously threaten human health and biological systems [8]. These metals gain their danger from their characteristic of bioaccumulation, which causes severe health consequences, including kidney failure, nervous system damage, and cancer formation [9]. Although Fe is an essential element for life, high levels in water resulting from various activities cause health problems such as gastrointestinal disorders and tissue poisoning, especially in rural areas with limited infrastructure. As for Cd, it is classified as one of the most toxic metals, even at low concentrations, as long-term exposure to it is associated with increased rates of lung and bone cancer [10].

■ EXPERIMENTAL SECTION

Materials

The following items have been purchased iron(II) chloride tetrahydrate ($FeCl_2·4H_2O$, 99.0%), cadmium chloride dihydrate, ($CdCl_2·2H_2O$, 99.0%), ethanol (C_2H_5OH, 99.5%), hydrochloric acid (HCl, 36.5–38.0%), and sodium hydroxide (NaOH, 99.0%), from the company Merck. All reagents were of analytical grade and used without further purification.

Instrumentation

The prepared oxides was recorded using the scanning electron microscope (FE-SEM, Festo, German), Energy-dispersive X-ray spectroscopy (EDX, Axia, PANalytical, German) in imaging the NPs. Brunauer-Emmett-Teller (BET, BEL Japan, INC), atomic absorption (Shimadzu AA 7000, Japan), FTIR spectroscopy (Shimadzu-1S, Japan), and X-ray diffraction (XRD, Aeris, PANalytical, Germany) were used in this study.

Procedure

Preparation of fig leaf powder

The plant extract was manufactured from the leaves of the fig tree after collecting the leaves and washing them well in two stages using both tap water and distilled water, followed by drying the leaves, then grinding the dried leaves into a fine powder, which was then subjected to sifting and preservation.

Synthesis of CuO NPs

The nanomaterial was prepared by following the green synthesis method, where an amount of 0.27 g of $CuCl_2$ aqueous salt was measured in a glass beaker, to which 400 mL of deionized water was added with continuous stirring until complete dissolution was achieved. Then, 10 mL of the plant extract was added while the mixture was stirred at room temperature. Followed by pH adjustment using a 1 M NaOH solution. A dark brown solid is obtained by filtration after the reaction. Then, it is washed with deionized water and ethanol to remove impurities before being placed in an oven at 60 °C to dry for 2 h [11].

Synthesis of ZnO NPs

The wet chemical method was used to synthesize and produce ZnO NPs by using a zinc nitrate hexahydrate ($Zn(NO_3)_2·6H_2O$) solution. The NaOH solution, 0.5 mol/L was prepared by dissolving 5 g of NaOH in 250 mL of deionized water and stirring the solution at 60 °C. The 0.5 mol/L $Zn(NO_3)_2$ solution was obtained by dissolving 37.175 g of $Zn(NO_3)_2·6H_2O$ in 250 mL of deionized water, which was then added dropwise to the alkaline solution. The resulting mixture was stirred and heated for 3 h. Upon reaction completion, the solution was allowed to settle for 10 min, followed by centrifugation at 10,000 rpm for 10 min, after which the NPs precipitates were washed 5 times with deionized water and dried at 70 °C. The ZnO NPs underwent complete conversion during the drying process, resulting in a white powder [12].

Preparation of composite

The ZnO NPs were added to 200 mL of ethanol in a shaking water bath for 1 h. The CuO NPs were added to 50 mL of ethanol, and the product was stirred using a shaking water bath for 1 h until equilibrium was achieved. Then, the CuO NPs added to ethanol were mixed with ZnO NPs in ethanol. The composite was stirred for 8 min and then stirred for 12 h. Finally, a centrifugation process at 2,000 rpm for 10 min was used to facilitate the separation. The resulting product was filtered, washed, and dried in an oven at 78 °C for 16 h. Finally, the dry residue was ground into a fine powder [13].

Characterization of NPs

The following imaging techniques have been used for NPs: the FE-SEM, EDX, FTIR, and XRD. Scherer's equation in Eq. (1) was used to calculate the mean crystal sizes (D) of the composite sample [14]. The equation was based on XRD data. The XRD instrument was used to analyze the data with a voltage of 40.0 kV, a wavelength of 0.1540, a speed of 12° min^{-1}, a current of 30 mA, and an angle range of 20–80°;

$$D = \frac{k\lambda}{\beta\cos\theta} \quad (1)$$

where θ = Bragg angle, λ = 0.1540 nm, β = full width half-maxima (FWHM), and k = the Scherrer constant with a value of 0.94.

Adsorption studies

Stock solutions of Cd(II) and Fe(II) ions were prepared by dissolving appropriate specified amounts of their salts in 1000 mL of distilled water. Different concentrations of metal ions, 5–40 mg L^{-1}, were prepared from stock solutions by dilution. In all experimental work, a precisely weighed amount of the nanocomposite was added to 100 mL of aqueous solution in a 250 mL flask. Then the solution was mixed in a rotary shaker. The samples were analyzed after the filtration. The results obtained were used to calculate the heavy metal removal percentage (R%) [15], and the equilibrium capacity (q_e) [16], of Cd(II) and Fe(II) ions using an AA and using the relationships shown in the Eq. (2) and (3);

$$R\% = \frac{C_0 - C_e}{C_0} \times 100\% \quad (2)$$

$$qe = \frac{C_0 - C_e}{m} \times V \quad (3)$$

where q_e is the equilibrium capacity of the nanoadsorbent (mg g^{-1}), C_0 is the initial concentration for the heavy metal (mg L^{-1}), C_e is concentration at equilibrium for the heavy metal (mg L^{-1}), V is volume of solution (L), and m is adsorbent weight (g).

■ RESULTS AND DISCUSSION

Characterization of NPs

FE-SEM

An FE-SEM test was performed on the CuO/ZnO NPs composite . This methodology is commonly used to analyze nanomaterials with exceptional accuracy. It is an effective technique for investigating NPs' crystalline form and elucidating its external structural surface composition, dimensions, distribution, and shape [17]. The FE-SEM image of the sample in Fig. 1 shows that the nanocomposite pattern consists of numerous spherical CuO and ZnO particles, clearly demonstrating the composite surface structure of the two nanomaterials. The small ZnO NPs adhere to the CuO substrate, which improves surface properties and removal characteristics.

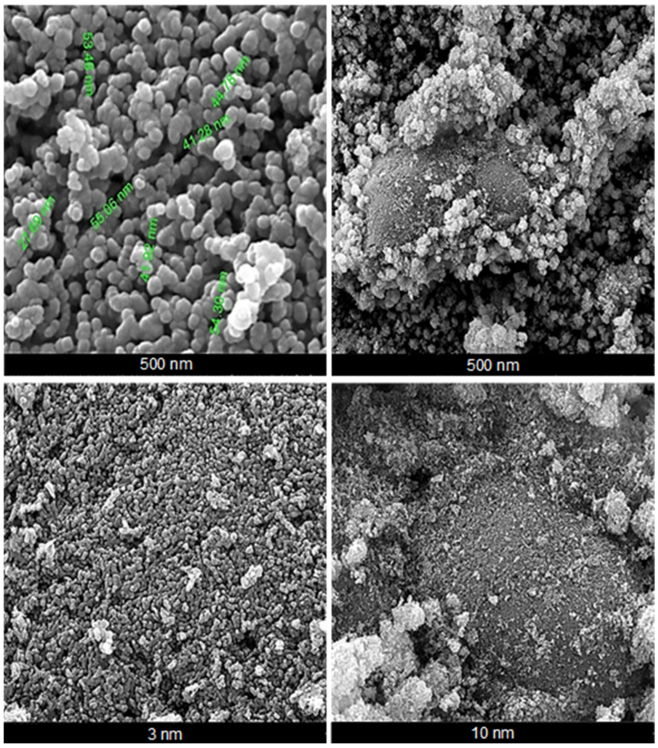

Fig 1. FE-SEM image of CuO/ZnO NPs composite

EDX analysis

An EDX analysis showed oxygen (O) at 52.2%,. Copper (Cu) was observed at 24.3% atomic weight, and zinc (Zn) appeared at 23.5%. The reason that only O, Cu, and Zn appeared in the analysis, while other elements (such as carbon or hydrogen) did not appear, is due to the purity of the materials initially prepared, the absence of impurities or organic bonds in the sample after the purification process (washing with water and ethanol), and the sensitivity of the device, which may not detect elements of trace levels.

The results show that Cu and Zn have similar weight ratios and that the high O concentration in the sample. Furthermore, the errors (atomic error ≤ 0.8%) indicate a high accuracy in the measurements, as shown in the Table 1, enhancing the reliability of the results, based on the quantities used of both CuO and ZnO NPs in a 1:1 ratio. The high performance in adsorption of Fe(II) and Cd(II) ions is attributed to the properties of the composite, such as its surface area, and the synergistic interaction between the two components, which increases adsorption efficiency. These results show

Table 1. Elements present in the nanocomposite sample and their percentage

Element	%Atomic	%Atomic error	%Weight	%Weight error
O	52.2	0.8	21.4	0.3
Cu	24.3	0.3	39.4	0.5
Zn	23.5	0.4	39.3	0.6

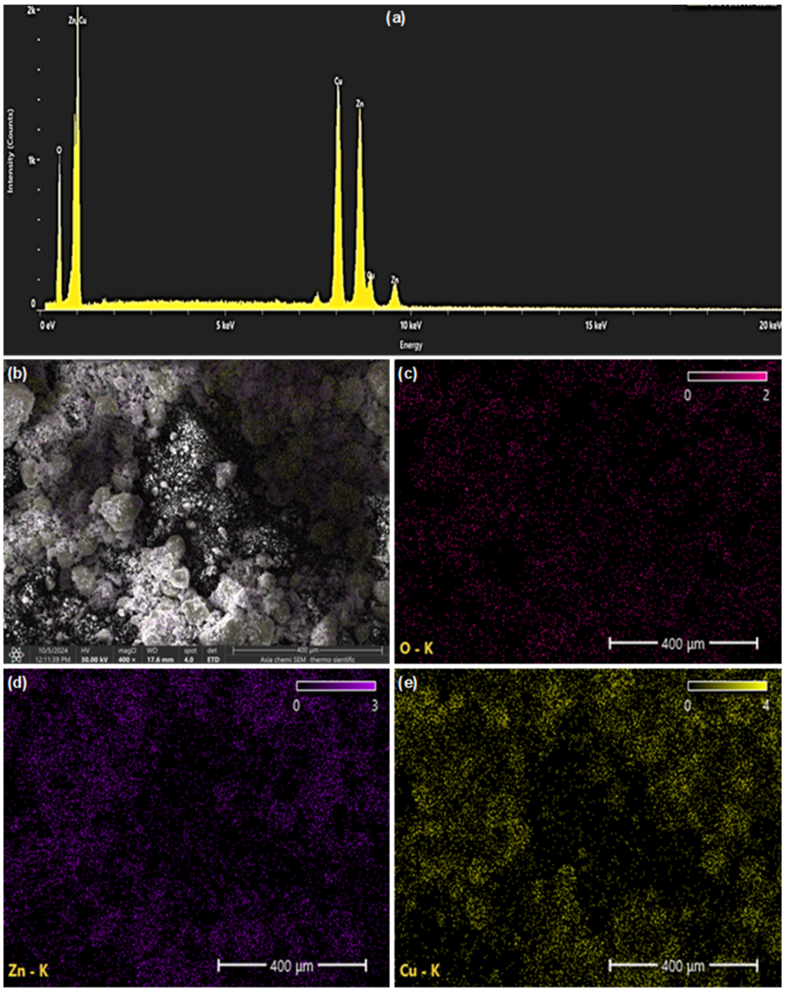

Fig 2. (a) Elements present in the sample, and (b, c, d, e) map EDX image of elements in CuO/ZnO NPs

similarity with the study that used the CuO/ZnO nanocomposite in dye removal, confirming the superiority of the composite in the current study compared to using CuO only, as in the study. Analysis at a 400 µm scale via (Fig. 2) demonstrates that Zn and O exist in a uniform distribution across the sample surface to form ZnO [18].

FTIR analysis

The FTIR spectra of composite CuO/ZnO NPs were obtained using CsI powder in the form of a disc in the range 250–4000 cm^{-1}. The CuO/ZnO spectra in Fig. S1 show that the essential peaks as a stretching vibration of the O–H around 3634–3403 cm^{-1}, the C–H group at 1465 cm^{-1}, the strong Zn–O band around 393–440 cm^{-1}, and the strong Cu–O band around 517–570 cm^{-1}. Hence, the results referred to ZnO and CuO creation [19].

BET analysis

The data presented reflect an analysis of the adsorption and porosity properties of a sample containing ZnO and CuO in a nanocomposite using nitrogen adsorption at 77 K (Fig. S2(a)). The BET model is used to generate the adsorption curve. The adsorbed gas's high value indicates a large surface area and high surface activity. The properties of the synthesized compounds were determined. The specific surface area (S) was calculated using the Eq. (4) [20], which was 13.372 m^2/g. This is due to the nanostructure or high porosity, which provides effective binding sites for adsorbed molecules. The Barrett-Joyner-Halenda (BJH) is shown in Fig. S2(b). Pore distribution analysis calculates the pore size distribution based on relative vapor pressure. The curve shows a multi-size distribution of pores. This wide pore distribution is due to the crystal structure, which creates a variety of pores during synthesis. Thus, these properties give the nanocomposite a high surface area and multi-size pore distribution, which makes it a suitable adsorbent for pollutants on its active surface. The result was almost identical when compared with a hydrothermally manufactured sample [21].

$$S = \frac{V_m \cdot N_A \cdot \sigma}{V_{mol}} \tag{4}$$

where V_m is the volume of gas adsorbed to form a monolayer and its value 4.8150 cm^3/g, N_A is Avogadro's number, σ is cross-sectional area of nitrogen molecule (16.2×10^{-20} m^2), and V_{mol} is the gas molar volume at standard conditions (22.4 dm^3/mol).

XRD analysis

The XRD technique was used to analyze the crystal structure of the CuO/ZnO NPs composite. According to XRD diffractograms, the main peaks the diffraction intensity are indicated at 36.24°, 35.50°, 38.71°, 34.40°, 31.76°, 67.95°, 56.58°, 62.83°, and 48.76°, corresponding to the (101), (−111), (111), (002), (100), (112), (110), (103), and (202) planes of nanocomposite. These peaks indicating the presence different crystalline phases in the sample, which shown in Fig. S3. The detected distinct crystalline patterns because of peaks matching both CuO and ZnO. These results confirm the presence of both crystal types in the nanocomposite. They are in remarkable agreement with recent studies [22], confirming the successful synthesis of the sample's CuO/ZnO double crystal structure.

Factors Affecting the Adsorption Process by Nanocomposite

Effect of pH

To identify the optimum pH that helps increase the adsorption process, Fig. 3 shows the effect of changing pH on removing Cd(II) and Fe(II) ions. The removal efficiency is maximum at pH = 6 for both ions, with some superiority having been observed in the removal of Cd(II), 86.7%, compared to Fe(II), 84.9%. The study was conducted using different solutions ranging from 2–11 at a controlled temperature of 25 °C for 50 min periods for both ions, using a sorbent dose of 0.09 g and an initial concentration of 10 mg L^{-1}. The adsorption capacity showed a clear difference upon increasing the pH, reaching a maximum of 6 for both ions. This indicates that the removal efficiency and adsorption capacity were significantly improved upon raising the pH, and the

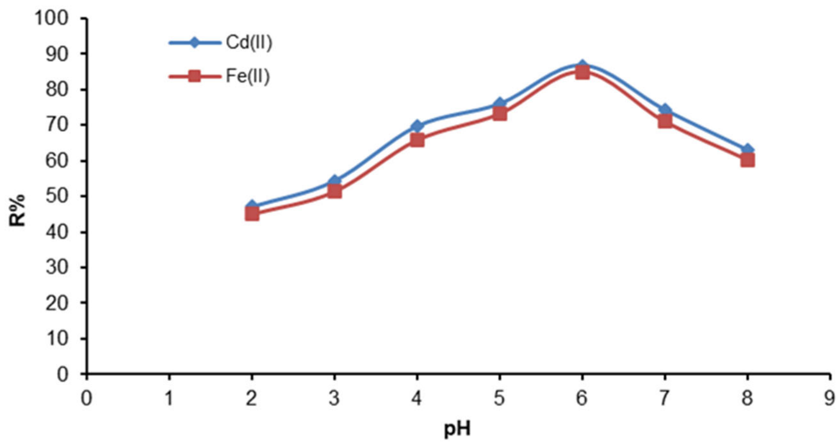

Fig 3. The effect of changing pH on the removal of Cd(II) and Fe(II) by a composite

surface of the nanomaterial is likely to be protonated, leading to increased competition between H^+ ions and heavy metals for the available adsorption sites. The competition between H^+ ions decreases the efficiency of adsorption because they bind more tightly to sites than heavy metal ions do. However, with increasing pH, deprotonation of the Nano surface occurs, facilitating the ionization of active groups such as HO^- groups. The ionized functional groups on polymeric membranes create strong binding sites that enhance the adsorptive capacity for ions. Furthermore, increasing pH corresponds to a decrease in the positive surface charge, thus reducing the repulsion between charged ions and the nano-surface. This decrease in repulsion allows more ions to approach and adhere to the nano-surface, increasing the adsorption mechanism [23].

Effect of contact time

The effect of contact time shown in Fig. 4 on the adsorption of Cd(II) and Fe(II) ions by CuO/ZnO NPs at 25 °C, heavy metal concentration 10 mg L^{-1} and adsorbent weight of 0.09 g. It is observed that the removal rate of heavy metals increases with the increase of contact time until the equilibrium state between the heavy metal ions on the nanomaterial and those remaining in the solution is reached. This phenomenon may be attributed to the saturation of the nanomaterial surface with heavy metal ions. The adsorption rate shows an ascending trend as the contact time extends from 10 to 80 min. Therefore, it can be concluded that the concentration of adsorbed heavy metal ions gradually increases until reaching the equilibrium point, which shows a slight decrease with time. The optimum contact time was determined to be 40 min for both types of ions. The maximum removal was 86.1% for Cd(II) and 83.2% for Fe(II), which was a slight superiority Cd(II). This result indicates that the adsorption process has an endothermic property. The graphical representation of the removal rate of heavy metals with time is characterized by curves, which eventually lead to saturation.

Effect of initial concentration

The effect of the initial concentration on the removal of heavy metal ions and a demonstration of the effect of changing the concentration on the removal of Cd(II) and Fe(II) ions is shown in Fig. 5 by CuO/ZnO NPs, at 25 °C, pH = 6, contact time 40 min and the weight of the adsorbent is 0.09 g. The maximum removal was 86.5% for Cd(II) and 84.3% for Fe(II), which was a slight superiority Cd(II). We noticed that the highest adsorption was at 10 mg L^{-1}, and after this concentration, the adsorption began to decrease. This is due to the number of active and effective sites available on the surface of the nanocomposite on which adsorption occurs. When the concentration of metals increases, the number of these active sites becomes saturated with pollutants quickly, which leads to the adsorption rate of pollutants decreasing compared to increasing the concentration of ions in the solution. The results are consistent with the general trend in recent research [24], where nanocomposites have high efficiency in high adsorption capacity for heavy metals.

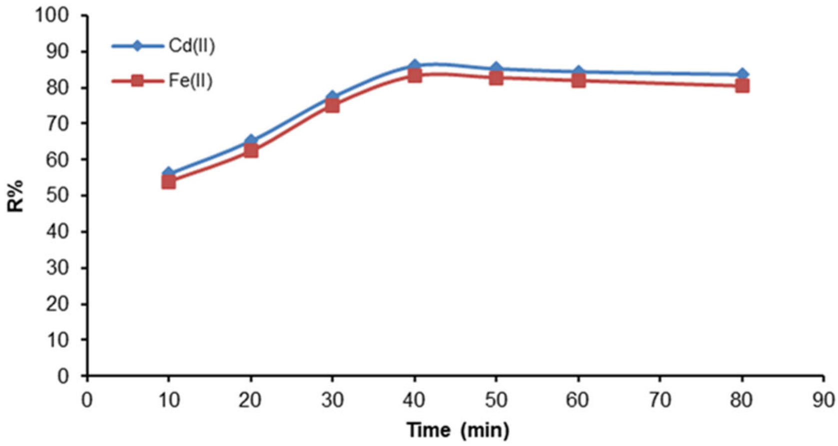

Fig 4. The effect of time on the removal of Cd(II) and Fe(II) by a composite

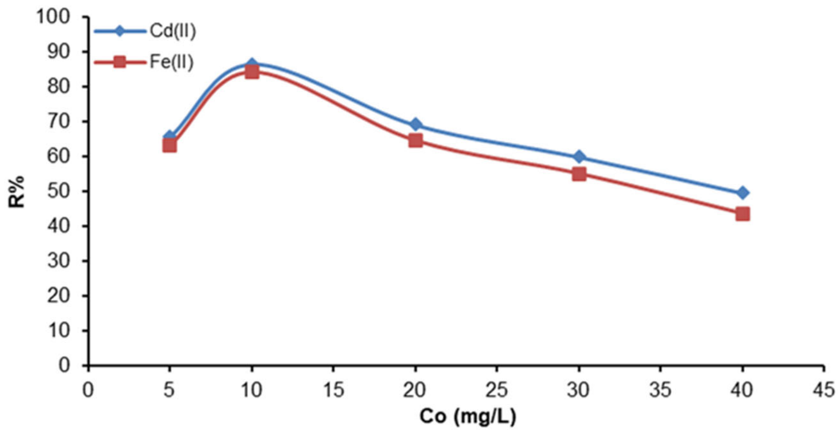

Fig 5. The effect of initial concentration on the removal of Cd(II) and Fe(II) by a composite

Effect of adsorbent dose

The effect of changing the sorbent dosage is significant. It plays an effective role in the removal of Cd(II) and Fe(II) ions by CuO/ZnO composite at 25 °C, pH = 6, initial concentration 10 mg L^{-1}, and sorbent weight 0.09 g. This could be due to several reasons, including the aggregation or interaction of the adsorbent molecules with each other. Thus, the active sites become unavailable because the same adsorbent molecules block them, or the adsorbent molecules compete for the same sites, or it could be due to the rate of diffusion of heavy metals to the active sites on the surface being low, or the solution reaching a state of equilibrium between the amount of pollutants on the surface and those that are free in the solution. In all previous cases, increasing the dose does not significantly affect adsorption [25]. The Fig. 6 shows the process of absorbing and removing heavy metal ions, which shows the result of changing the sorbent dosage. Some superiority has been observed in the removal of Cd(II), 86.3%, compared to Fe(III), 84.2%.

Adsorption isotherms

The adsorption curve in Fig. 7 showed saturation when the initial concentration of heavy metal ions increased, as the active and active sites for adsorption on the surface were saturated very quickly until the maximum adsorption capacity was reached, where the highest adsorption efficiency reached 86.7 and 84.9% for both Cd(II) and Fe(III), respectively, indicating that the active sites for adsorption have a greater tendency and affinity to adsorption of Cd(II), and this is consistent with the assumption that the active sites are homogeneous and have equal binding energy [26].

Langmuir and Freundlich model

According to the Langmuir model, the coefficient of determination R^2 = 0.9953 for the adsorption of Cd(II)

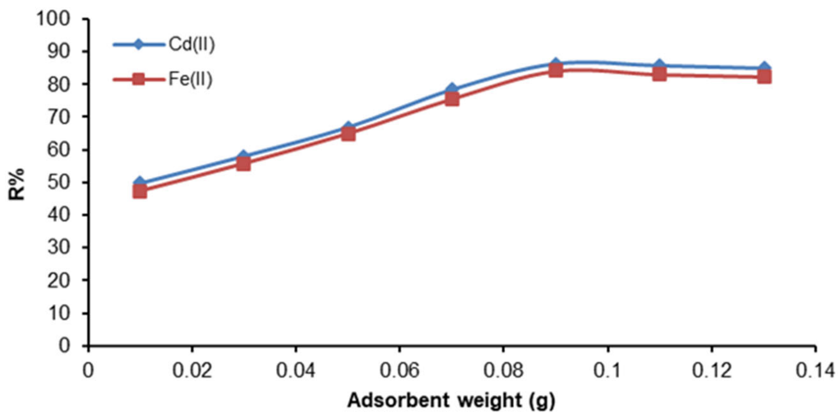

Fig 6. The effect of adsorbent weight on the removal of Cd(II) and Fe(II) by a composite

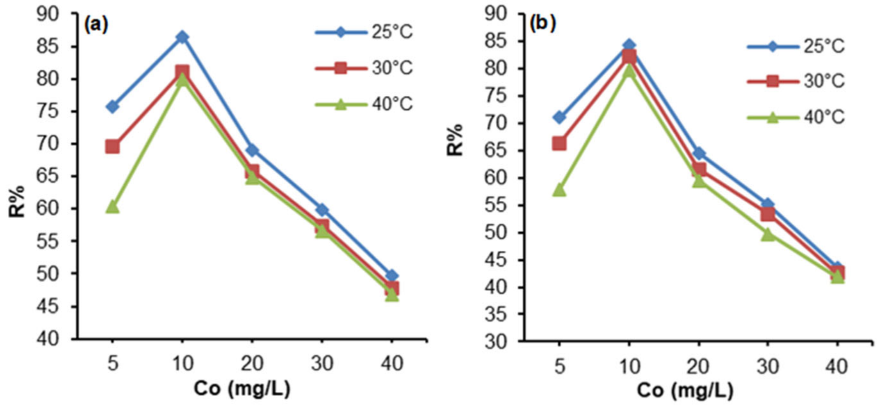

Fig 7. The adsorption isotherms of heavy metals by a composite NPs (a) Cd(II) and (b) Fe(II)

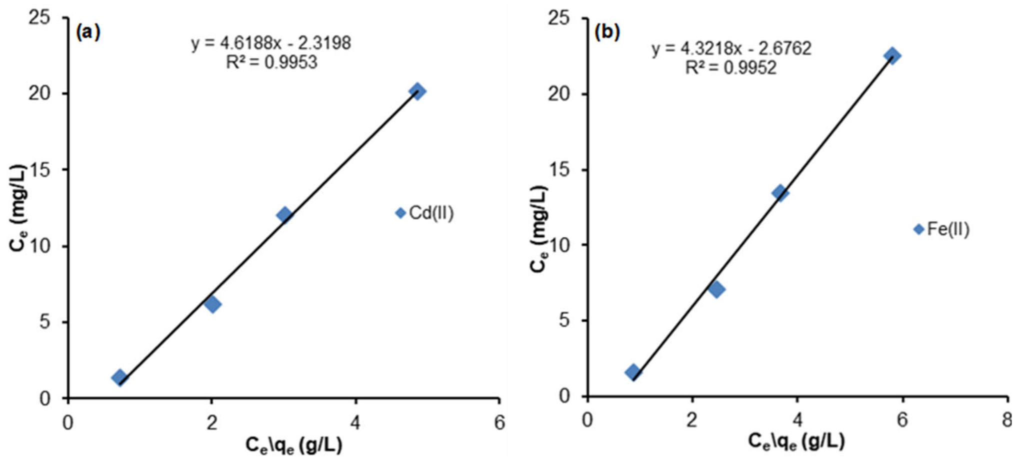

Fig 8. Langmuir plot of composite NPs for (a) Cd(II) and (b) Fe(II) removal at 25 °C

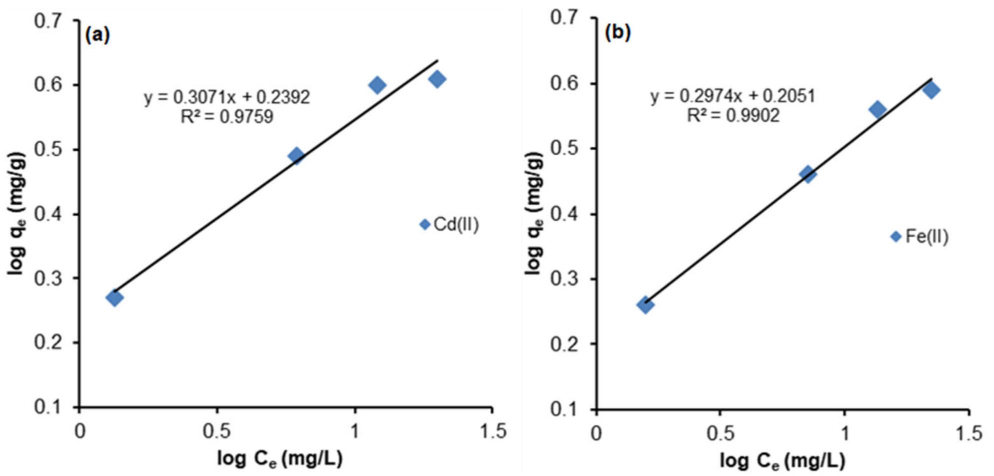

Fig 9. Freundlich plot of composite NPs for (a) Cd(II) and (b) Fe(II) removal at 25 °C

ions and R^2 = 0.9952 for Fe(II) ions are shown in Fig. 8. The observed high R^2 values confirm that experimental results match well with the theoretical assumptions behind the Langmuir model of uniform surface adsorption with identical active sites [27]. Meanwhile, in the Freundlich model shown in Fig. 9, R^2 = 0.9759 for Cd(II) and R^2 = 0.9902 for Fe(II). Although these values are high, they are lower than the Langmuir model, indicating that the assumption of a heterogeneous (multilayered) surface is less accurate in describing the adsorption mechanism in this case [28].

Based on the higher coefficients of determination R^2 and its proximity to the ideal value of 1, the Langmuir model is considered more accurate and suitable for explaining the adsorption process of Cd(II) and Fe(II) ions on the nanocomposite surface, The data support monolayer adsorption of a homogeneous system rather than the more complex adsorption process, which involves multiple layers. This is due to the high percentage of heavy metal adsorption, 86.7% for Cd(II) and 84.9% for Fe(II), which is consistent with the assumption of saturation of the active sites on the surface. The results from XRD analysis (Fig. S3), FE-SEM (Fig. 1), and BET analysis (Fig. S2) validate the assumptions made by Langmuir, thus verifying the homogeneous crystal structure and uniform nanoparticle arrangement.

Kinetic Studies

The quasi-second-order model best explains the adsorption dynamics because the process depends on chemical interactions on the adsorbent's surface when applying the mathematical operations of the two models. R^2 = 0.983 for Cd(II), and R^2 = 0.973 for Fe(II), Higher than the semi-first class model R^2 = 0.923 for Cd(II) and R^2 = 0.908 for Fe(II), as shown in Fig. 10. The high adsorption efficiency reflects the interconnected interactions between the nanocomposite components and their structural properties, as chemical bonds are formed between the ions and the nanocomposite surface (e.g., ion exchange or surface interactions). The ZnO particles enhance the activity of CuO by increasing active sites and reducing particle aggregation. Furthermore, the results are consistent with the Langmuir model ($R^2 \approx$ 0.995), supporting the adsorption happens in a homogeneous monolayer. This result is consistent with previous studies [29-30]. These results support using this material as a promising solution for treating water contaminated with heavy metals [31].

■ CONCLUSION

The experimental results presented in this study indicate the high adsorption efficiency shown by the nanomaterial's in removing these pollutants. The results of adsorption of heavy metal ions by the nanocomposite were arranged as follows: Cd(II) > Fe(II). The important factors that played a major role in the removal process were pH, time, and concentration. This material's economic and profile represents an important solution model in removing pollutants by using environmentally friendly methods to prepare nanomaterial and increasing the adsorption efficiency when creating a nanocomposite consisting of more than one nanomaterial. The expanding applications of this material include removing other pollutants that are harmful to the environment, improving the properties by studying some modifications to the adsorption surface to increase the adsorption efficiency, and understanding the mechanism of pollutant diffusion on the surface during

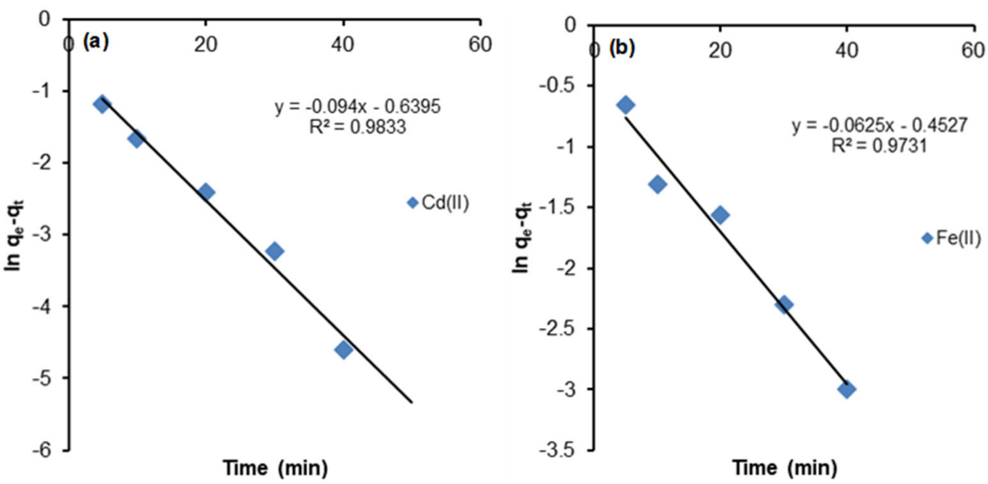

Fig 10. Kinetic parameters for adsorption of Cd(II) and Fe(II) by composite NPs

the adsorption process. This study confirms the possibility of nanocomposite materials based on the use of metal oxides, a promising and effective method to reduce and remove water pollutants, with the possibility of developing and expanding its use.

■ CONFLICT OF INTEREST

The authors state that conflicts of interest do not exist regarding this paper's publication.

■ AUTHOR CONTRIBUTIONS

Mohammed Khlaif Challab, Mohammed Turki Khathi, and Mohammad Javad Chaichi conceived the manuscript, developed the methodology, wrote it, and revised it. Mohammed Khlaif Challab conducted the experiment. Omleila Nazari and Shahram Ghasemi developed the methodologies and validated the manuscript. All authors approved the final version of this manuscript.

■ REFERENCES

[1] Al-Ghanimi, B.K., Abd Nusaif, K.I., and Al-Baiati, M.N., 2025, Novel nano chitosan loaded with amoxicillin as inhibitor lung cancer cell line (A549): Biological activity and molecular studies, *Moroccan J. Chem.*, 13 (2), 480–494.

[2] Abdulnabi, O.W., Alsalame, H.A.A., and AL-Baiati, M.N., 2025, Preparation and characterization a nano chitosan-mefenamic acid composites as biocompatible treatment anti-colon cancer cell line HCT-29, *Moroccan J. Chem.*, 13 (1), 366–380.

[3] Shinde, S., Parjane, S., Turakane, H., Basnet, P., Oza, R., Abhale, Y., and Ghotekar, S., 2023, Bio-inspired synthesis and characterizations of groundnut shells-mediated $Cu/CuO/Cu_2O$ nanoparticles for anticancer, antioxidant, and DNA damage activities, *J. Sol-Gel Sci. Technol.*, 106 (3), 737–747.

[4] Sukumar, S., Rudrasenan, A., and Padmanabhan Nambiar, D., 2020, Green-synthesized rice-shaped copper oxide nanoparticles using *Caesalpinia bonducella* seed extract and their applications, *ACS Omega*, 5 (2), 1040–1051.

[5] Choudhary, N., Chaudhari, J., Mochi, V., Patel, P., Ali, D., Alarifi, S., Sahoo, D.K., and Yadav, V.K., 2023, Phytonanofabrication of copper oxide from *Albizia saman* and its potential as an antimicrobial agent and remediation of Congo red dye from wastewater, *Water*, 15 (21), 3787.

[6] Jabeen, S., Siddiqui, V.U., Bala, S., Mishra, N., Mishra, A., Lawrence, R., Bansal, P., Khan, A.R., and Khan, T., 2024, Biogenic synthesis of copper oxide nanoparticles from *Aloe vera*: Antibacterial activity, molecular docking, and photocatalytic dye degradation, *ACS Omega*, 9 (28), 30190–30204.

[7] Challab, M.K., 2024, Removal of Pb(II) and Cu(II) from water using silver nanoparticles prepared using extract plant (*Albizia odoratissima*), *Al-Qadisiyah J. Pure Sci.*, 29 (1), 11.

[8] Chan, Y.B., Aminuzzaman, M., Win, Y.F., Djearamane, S., Wong, L.S., Guha, S.K., Almohammadi, H., Akhtaruzzaman, M., and Tey, L.H., 2024, *Garcinia mangostana* L. leaf-extract-assisted green synthesis of CuO, ZnO and CuO-ZnO nanomaterials for the photocatalytic degradation of palm oil mill effluent (POME), *Catalysts*, 14 (8), 486.

[9] Malvandi, H., 2024, Metals concentration and human health risk assessment in some fish species from the southern Caspian Sea, *Mar. Pollut. Bull.*, 202, 116336.

[10] Charkiewicz, A.E., Omeljaniuk, W.J., Garley, M., and Nikliński, J., 2025, Mercury exposure and health effects: What do we really know?, *Int. J. Mol. Sci.*, 26 (5), 2326.

[11] Hassan, K.H., Saadi, S.K., Jarullah, A.A., and Harris, P., 2018, Green synthesis and structural characterisation of CuO nanoparticles prepared by using fig leaves extract, *Pak. J. Sci. Ind. Res., Ser. A*, 61 (2), 59–65.

[12] Hamouda, R.A., Yousuf, W.E., Mohammed, A.B.A., Mohammed, R.S., Darwish, D.B., and Abdeen, E.E., 2020, Comparative study between zinc oxide nanoparticles synthesis by biogenic and wet chemical methods *in vivo* and *in vitro* against *Staphylococcus aureus*, *Microb. Pathog.*, 147, 104384.

[13] Bagheri, A.R., Ghaedi, M., Asfaram, A., Bazrafshan, A.A., and Jannesar, R., 2017, Comparative study on

ultrasonic assisted adsorption of dyes from single system onto Fe_3O_4 magnetite nanoparticles loaded on activated carbon: Experimental design methodology, *Ultrason. Sonochem.*, 34, 294–304.

[14] Aziz, S.M.A., Nayef, U.M., and Rasheed, M., 2025, Synthesis of CuO@ZnO nanoparticle core–shell formed via laser ablation in liquid for photocatalytic applications, *Plasmonics*, 20 (5), 2595–2605.

[15] Mahmoud, M.E., Kamel, N.K., Amira, M.F., and Fekry, N.A., 2024, Nitrate removal from wastewater by a novel co-biochar from guava seeds/beetroot peels-functionalized-Mg/Al double-layered hydroxide, *Sep. Purif. Technol.*, 344, 127067.

[16] N'Dah, F.M., N'diaye, A.D., Ech-chihbi, E., Azzaoui, K., Sabbahi, R., Siaj, M., and Kankou, M., 2024, Kinetics and equilibrium study for the adsorption of Maxilon blue dye on *Prosopis juliflora* fruit seeds as a low-cost adsorbent, *Moroccan J. Chem.*, 12 (3), 1042–1057.

[17] Jeevarathinam, M., and Asharani, I.V., 2024, Synthesis of CuO, ZnO nanoparticles, and CuO-ZnO nanocomposite for enhanced photocatalytic degradation of Rhodamine B: A comparative study, *Sci. Rep.*, 14 (1), 9718.

[18] Ullah, S., Aqsa Batool Bukhari, S., Nasir, H., Akhtar, T., Mahboob, S., and Zahid, M., 2024, Efficient photocatalytic degradation of profenofos by CuO-ZnO nanocomposite, *J. Photochem. Photobiol., A*, 455, 115787.

[19] Messai, R., Ferhat, M.F., Belmekki, B., Alam, M.W., Al-Othoum, M.A.S., and Sadaf, S., 2024, GAD plasma-assisted synthesis of ZnO nanoparticles and their photocatalytic activity, *Mater. Res. Express*, 11 (1), 015006.

[20] Irwansyah, F.S., Amal, A.I., Diyanthi, E.W., Hadisantoso, E.P., Noviyanti, A.R., Eddy, D.R., and Risdiana, R., 2024, How to read and determine the specific surface area of inorganic materials using the Brunauer-Emmett-Teller (BET) method, *ASEAN J. Sci. Eng.*, 4 (1), 61–70.

[21] Yang, H., Zhao, Y., Guo, Y., Wu, B., Ying, Y., Sofer, Z., and Wang, S., 2024, Surfactant-mediated crystalline structure evolution enabling the ultrafast green synthesis of bismuth-MOF in aqueous condition, *Small*, 20 (15), 2307484.

[22] Hosseini, R., Sayadi, M.H., and Shekari, H., 2019, Adsorption of nickel and chromium from aqueous solutions using copper oxide nanoparticles: Adsorption isotherms, kinetic modeling, and thermodynamic studies, *Avicenna J. Environ. Health Eng.*, 6 (2), 66–74.

[23] Mahmoud, E.R.I., Aly, H.M., Hassan, N.A., Aljabri, A., Khan, A.L., and El-Labban, H.F., 2024, Biochar from date palm waste via two-step pyrolysis: A modified approach for Cu(II) removal from aqueous solutions, *Processes*, 12 (6), 1189.

[24] Tenea, A.G., Dinu, C., Rus, P.A., Ionescu, I.A., Gheorghe, S., Iancu, V.I., Vasile, G.G., Pascu, L.F., and Chiriac, F.L., 2024, Exploring adsorption dynamics of heavy metals onto varied commercial microplastic substrates: Isothermal models and kinetics analysis, *Heliyon*, 10 (15), e35364.

[25] Meena, A.K., Kadirvelu, K., Mishra, G.K., Rajagopal, C., and Nagar, P.N., 2008, Adsorptive removal of heavy metals from aqueous solution by treated sawdust (*Acacia arabica*), *J. Hazard. Mater.*, 150 (3), 604–611.

[26] El Bourachdi, S., El Ouadrhiri, F., Moussaoui, F., Saleh, E.A.M., El Amri, A., Althomali, R.H., Kassem, A.F., Moharam, M.M., Ayub, A.R., Husain, K., Hassan, I., and Lahkimi, A., 2024 Enhancing graphene oxide production and its efficacy in adsorbing crystal violet: An in-depth study of thermodynamics, kinetics, and DFT analysis, *Int. J. Chem. Eng.*, 2024 (1), 8222314.

[27] Bathula, C., Nissimagoudar, A.S., Kumar, S., Jana, A., Sekar, S., Lee, S., and Kim, H.S., 2024, Enhanced photodegradation of methylene blue by Zr-doped TiO_2: A combined DFT and experimental investigation, *Inorg. Chem. Commun.*, 164, 112442.

[28] Abdul Sattar, O.D., Mohd Khalid, R., and Yusoff, S.F.M., 2024, Optimizing methylene blue dye adsorption onto liquid natural rubber-based hydrogel: Kinetics, isotherms and reusability, *Sains*

Malays., 53 (5), 1149–1166.
[29] Fathi, A.G., Abdelrahman, E.A., Abou-Krisha, M.M., Shah, R.K., Saad, F.A., and El Rayes, S.M., 2025, Facile Synthesis of novel nanocomposite consists of β-FeOOH, chitosan, and salicylaldehyde for efficient removal of Zn(II) ions from aqueous media, *J. Inorg. Organomet. Polym. Mater.*, s10904-025-03653-3.
[30] Aguilar, N., Rozas, S., Escamilla, E., Rumbo, C., Martel, S., Barros, R., Marcos, P.A., Bol, A., and Aparicio, S., 2024, Theoretical multiscale study on the properties, aqueous solution behavior and biological impact of zinc oxide nanoparticles, *Surf. Interfaces*, 46, 103965.
[31] Kataria, N., and Garg, V.K., 2018, Optimization of Pb(II) and Cd(II) adsorption onto ZnO nanoflowers using central composite design: Isotherms and kinetics modelling, *J. Mol. Liq.*, 271, 228–239.